Effect of gain anisotropy on low-frequency dynamics in four-level solid-state lasers

Jong-Dae Park[1], Aaron M[c]Kay[2] and Judith M. Dawes[2*]

[1]*Department of Physics, Pai-Chai University, Daejon, Korea 302-735.*
[2]*Department of Physics, Macquarie University, Sydney, NSW 2109, Australia*
**Corresponding author: judith.dawes@mq.edu.au*

Abstract: Our anisotropic rate equation model outlines the relationship between the relaxation dynamics in a four-level solid-state laser and its anisotropic gain properties. Anisotropic pump rates and stimulated emission cross-sections were included to account for specific atom orientations in the gain material. The model is compared with experimental measurements of two relaxation oscillation frequencies which are related to the anisotropic atom-laser interaction in orthogonally polarized dual-mode lasers. The model predicts that crystal orientation and pump polarization affect the laser operation characteristics, as found experimentally. The gain anisotropy influences the fast laser dynamics, as in single-mode relaxation oscillations.

OCIS codes: (140.3580) Lasers, solid-state; (140.3430) Lasers, theory; (140.3530) Lasers, neodymium.

References and links

1. C. L. Tang, H. Statz, and G. deMars, "Spectral output and spiking behavior of solid-state lasers," J. Appl. Phys. **34**, 2289–2295 (1963).
2. K. Wiesenfeld, C. Bracikowski, G. James, and R. Roy, "Observation of anti-phase state in a multimode laser," Phys. Rev. Lett. **65**, 1749–1752 (1990).
3. K. Otsuka, P. Mandel, S. Bielawski, D. Derozier, and P. Glorieux, "Alternate time scale in multimode lasers," Phys. Rev. A **46**, 1692–1695 (1992).
4. S. Bielawski, D. Derozier, and P. Glorieux, "Anti-phase dynamics and polarization effects in the Nd-doped fiber laser," Phys. Rev. A **46**, 2811–2822 (1992).
5. T. Hill, L. Stamatescu, and M. W. Hamilton, "Method for determining anti-phase dynamics in a multimode laser," Phys. Rev. E. **61**, R4718–R4721 (2000).
6. A. McKay, P. Dekker, D. W. Coutts, and J. M. Dawes, "Enhanced self-heterodyne performance of dual-polarization lasers using a Nd-doped ceramic YAG laser," Opt. Commun. **272**, 425–430 (2007).
7. A. McKay, J. M. Dawes, and J. D. Park, "Polarization-mode coupling in (100)-cut Nd:YAG," Opt. Express **15**, 16342–16347 (2007).
8. Q. Zhang, B. Feng, D. Zhang, P. Fu, Z. Zhang, Z. Zhao, P. Deng, J. Xu, X. Xu, Y. Wang, and X. Ma, "Anti-phase state in a passively Q-switched Yb:YAG microchip multimode lasers with a saturable absorber GaAs," Phys. Rev. A **69**, 053815(2004).
9. M. Brunel, A. Amon, and M. Vallet, "Dual-polarization microchip laser at 1.53 µm," Opt. Lett. **30**, 2418–2420 (2005).
10. C. Masoller, M. S. Torre, and P. Mandel, "Anti-phase dynamics in multimode semiconductor lasers with optical feedback," Phys. Rev. A **71**, 013818 (2005).
11. B. Peters, J. Hunkemeier, V. M. Baev, and Y. I. Khanin, "Low-frequency dynamics of a Nd-doped glass laser," Phys. Rev. A **64**, 023816 (2001).
12. M. Sargent, III, M. O. Scully, and W. E. Lamb, *Laser Physics* (Addison-Wesley, Massachusetts, 1974).
13. M. Alouini, F. Bretenaker, M. Brunel, A. Floch, M. Vallet, and P. Thony, "Existence of two coupling constants in microchip lasers," Opt. Lett. **25**, 896–898 (2000).
14. E. Lacot and F. Stoeckel, "Nonlinear mode coupling in a microchip laser," J. Opt. Soc. Am. B **13**, 2034–2040 (1996).
15. P. Dekker and J. M. Dawes, "Pulsed output from a dual-polarization cw diode-pumped Nd:YAG laser," J. Opt. Soc. Am. B **15**, 247–251 (1998).

16. G. Bouwmans, B. Segard, P. Glorieux, P. Khandokhin, N. Milovsky, and E. Shirokov, "Polarization dynamics of longitudinally monomode bipolarized solid-state lasers," Radiophys. Quantum Electron. **47**, 729–742 (2004).
17. I. V. Ievlev, P. A. Khandokhin, and E. Yu. Shirokov, "Polarization dynamics of single-longitudinal-mode Nd:YAG lasers with a weakly anisotropic cavity," Quantum Electron. **36**, 228–232 (2006).
18. K. Otsuka, "Oscillation properties of anisotropic lasers," IEEE J. Quantum Electron. **14**, 49–55 (1978).
19. H. Zeghlache and A. Boulnois, "Polarization instability in lasers. I. Model and steady states of neodymium-doped fiber lasers," Phys. Rev. A **52**, 4229–4242 (1995).
20. M. Brunel, O. Emile, M. Alouini, A. L. Floch, and F. Bretenaker, "Experimental and theoretical study of longitudinally monomode vectorial solid-state lasers," Phys. Rev. A **59**, 831–840 (1999).
21. P. A. Khandokhin, P. A. Mandel, I. V. Koryukin, B. A. Nguyen, and Y. I. Khanin, "Disappearance of relaxation oscillation frequencies in a multimode solid-state laser," Phys. Lett. A **235**, 248–252 (1997).
22. J. L. Wagener, D. G. Falquier, M. J. F. Digonnet, and H. J. Shaw, "A Mueller matrix formalism for modeling polarization effects in Erbium-doped fiber," J. Lightwave Technol. **16**, 200–206 (1998).
23. R. Dalgliesh, A. D. May, and G. Stephan, "Polarization states of a single-mode (microchip) Nd^{3+}:YAG laser-Part I: Theory," IEEE J. Quantum Electron. **34**, 1485–1492 (1998).
24. R. Dalgliesh, A. D. May, and G. Stephan, "Polarization states of a single-mode (microchip) Nd^{3+}:YAG laser-Part II: Comparison of theory and experiment," IEEE J. Quantum Electron. **34**, 1493–1502 (1998).
25. J. Degnan, "Theory of optimally coupled Q-switched lasers," IEEE J. Quantum Electron. **25**, 214–220 (1989).
26. R. Kawai, Y. Asakawa, and K Otsuka, "Simultaneous single-frequency oscillations on different transitions in laser-diode-pumped microchip LiNdP4O12 lasers" IEEE J Quantum Electron. **35**, 1542-1547 (1999).
27. K. J. Weingarten, B. Braun, and U. Keller, "*In situ* small-signal gain of solid-state lasers determined from relaxation oscillation frequency measurements," Opt. Lett. **19**, 1140–1142 (1994).

1. Introduction

Since the early days of lasers, rate equation models have been developed to explain experimental laser behavior. Tang, Statz, and deMars (TSD) [1] were successful in explaining multimode phenomena such as anti-phase dynamics [2], relaxation oscillations (ROs) [3], and chaos [4]. The TSD rate equations considered spatial hole burning resulting from population inversion gratings created by standing waves. Collective behavior, self-organization and low frequency ROs result from spatial hole burning or cross-saturation in multi-longitudinal mode lasers. Anti-phase dynamics, typically attributed to spatial hole burning, have been observed in Nd:YAG [5–7], Yb:YAG [8], Er,Yb:glass [9] and semiconductor lasers [10], and in single- [6,7] and multi-longitudinal-mode lasers [11]. Multi-mode lasers also exhibit mode coupling [9,12–14]. Alouini *et al*. [13] observed mode coupling between different types of modes, i.e., between adjacent longitudinal modes and orthogonal polarizations. While longitudinal mode coupling has been explained using spatial overlap between competing modes, we consider polarization-mode coupling in the context of gain anisotropy in diode-pumped Nd:YAG lasers [15–17], following the work of Otsuka [18] on effects such as emission cross-section and fluorescence properties in strongly anisotropic Nd lasers. His rate equation model and experiments showed dual-polarization oscillations [18].

Polarization effects in solid-state lasers were considered by Zeghlache *et al*. [19], who assumed the existence of a transverse distribution of dipole moments, producing vectorial atomic polarizations. They assumed dipole moments of equal magnitudes along the atomic axes with random orientations. Brunel *et al*. [20] applied Zeghlache's approach [19] to explain nonlinear dynamics in dual-polarized microchip lasers from the interplay between the beat frequency and RO frequencies. Khandokhin *et al.* [21] observed low-frequency polarization dynamics in Nd-doped optical fiber lasers with elliptically polarized fields and randomly oriented dipoles. Wagener *et al*. [22] included the effect of gain anisotropy in erbium-doped fiber lasers with Mueller matrices. Dalgliesh *et al*. [23,24] used dipole moments aligned to 6 distinct atomic sites to model the polarization behavior of single-mode Nd:YAG lasers.

While Maxwell-Bloch equations explain the atom-laser interactions and anisotropic characteristics of solid-state lasers [23,24], they involve many variables with complex equations. The Maxwell-Bloch equations can be reduced to relatively simple rate equations

with proper approximations. For example, if the rate of change of atomic coherences in solid-state lasers is fast, then the atomic polarizations can be obtained as a function of the population difference between the upper and lower energy levels. For dual-orthogonally-polarized lasers, further simplifications can be made if the beat frequency is high compared to the inverse of the population inversion lifetime and if side-band frequencies generated by mode beating are not resonant with the laser cavity.

In this paper, we assume that such conditions are met, and present a rate equation model to account for the anisotropic laser-atom interactions. This model demonstrates that a second RO exists in dual-orthogonally-polarized lasers when the dipole moments are anisotropic. The crystal orientation and pump polarization (i.e., the gain anisotropy) also influence the RO frequencies. Experimental results illustrating the validity of the model and weak anisotropic effects in (111)-cut Nd:YAG laser material are also presented.

2. Anisotropic rate equations

Active atoms in crystalline solid-state lasers can be grouped into N atomic groups depending on the effective stimulated emission cross-sections [23], pumping rates and crystal symmetry. For simplicity, we assume that the laser eigen-polarization directions are pre-determined to be along the x and y axes by optical components inside the laser cavity. The anisotropic rate equations for the photon density ϕ_x for the x-polarized beam and ϕ_y for the y-polarized beam can be obtained by extending the four-level laser rate equations given by reference [25]

$$\frac{d\phi_x}{dt} = \frac{\phi_x}{t_r}\left[2l\left(\sum_{i=1}^{N}\sigma_x^i\left(n^i + n_x^i\right)\right) - \ln\left(\frac{1}{R}\right) - L_x\right] \tag{1}$$

$$\frac{d\phi_y}{dt} = \frac{\phi_y}{t_r}\left[2l\left(\sum_{i=1}^{N}\sigma_y^i\left(n^i + n_y^i\right)\right) - \ln\left(\frac{1}{R}\right) - L_y\right] \tag{2}$$

$$\frac{dn^i}{dt} = \beta\Lambda^i - \gamma c\left(\sigma_x^i\phi_x + \sigma_y^i\phi_y\right)n^i - \frac{n^i}{\tau_s} \tag{3}$$

$$\frac{dn_x^i}{dt} = \left(\frac{1-\beta}{2}\right)\Lambda^i - \gamma c\sigma_x^i\phi_x n_x^i - \frac{n_x^i}{\tau_s} \tag{4}$$

$$\frac{dn_y^i}{dt} = \left(\frac{1-\beta}{2}\right)\Lambda^i - \gamma c\sigma_y^i\phi_y n_y^i - \frac{n_y^i}{\tau_s} \tag{5}$$

where n^i is the shared population inversion between both orthogonal polarizations and n_x^i, n_y^i are polarized population inversions for each atomic group; t_r is the cavity round trip time; R, the output coupler reflectivity; L_x, L_y the cavity losses for x- and y-polarized beams, respectively; γ is the population inversion parameter, which is the change of the total population inversion due to stimulated emission of a photon [25] (γ=1 for four-level lasers); c is the velocity of light; τ_s is the lifetime of the population inversion; and β is the polarization mode overlap integral within the gain medium, which causes a population grating [1] in which the population inversion is shared by both polarizations. Λ^i is the pumping rate to the i-th group of atoms [7,23] which depends on the atomic orientations, the absorption cross sections along the specific atomic axis, and the pump laser polarization. In Nd:YAG, the active atoms can be divided into $N = 6$ groups according to their orientations and possible substitution sites in the YAG crystal. Pump diffusion and pump reabsorption also influence the laser dynamics [26], but we assume that these are small, and only consider effects of anisotropic interactions.

The effective stimulated emission cross-sections σ_x^i and σ_y^i for x- and y-polarized beams were calculated from stimulated emission cross-sections σ_q, σ_r, σ_s along the atomic axes $(\hat{q}, \hat{r}, \hat{s})$, using coordinate transformations from the atomic axis frame to the laboratory frame. The dipole moment ratios for Nd:YAG at the lasing wavelength (p_q:p_r:$p_s \equiv$ 4.0:1.3:4.1) and pump wavelength (p_q:p_r:$p_s \equiv$ 4.5:3.4:1.8) are from Refs. [23,24]. Absolute values of the

dipole moments were determined from the stimulated emission cross section ($\sigma = 2.8\times10^{-19}$ cm^2) and the ratio of dipole moments along the dipole axes of Nd:YAG. Steady-state photon densities and optical powers, and carrier densities for each group were found from the solutions of Eqs. (1)–(5). Figure 1(a,b) shows the calculated output power of a dual-mode Nd:YAG laser vs crystal orientation ϕ_c and relative pump polarization angle ϕ_p. The parameters used for the calculations (chosen for our experimental laser) were $R = 0.97$, $t_r = 267$ ps, $\gamma = 1$, $\tau_s = 230$ µs, $L_x = L_y = 0.06$, $l = 2$ mm, pump power 450 mW, pump beam diameter 200 µm and laser beam diameter 150 µm. We assumed $\beta \rightarrow 1$ due to strong polarization mode overlap effects from the co-located gain crystal and input mirror, and single longitudinal mode operation.

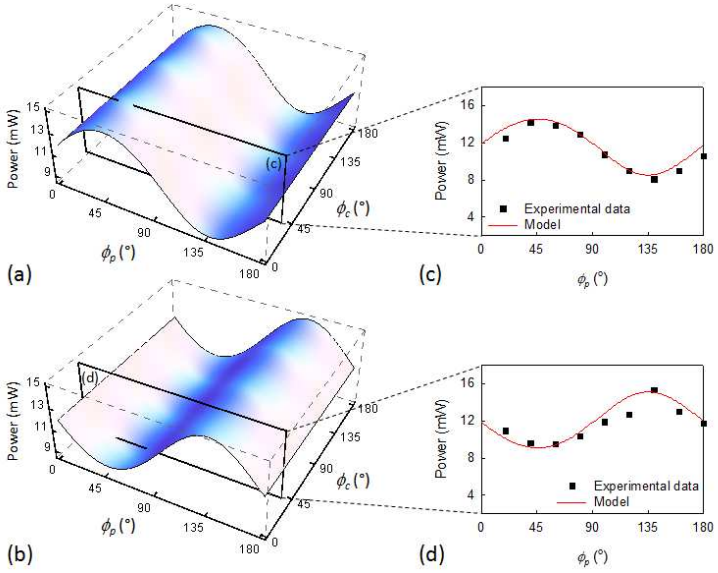

Fig. 1. Modeled (a) *x*- and (b) *y*-polarized output powers of a dual-polarization Nd:YAG laser pumped at 1.2 × threshold as a function of crystal angle (ϕ_c) and relative pump angle (ϕ_p). Corresponding experimental (c) *x*- and (d) *y*-polarized output powers as a function of pump polarization angle at a fixed crystal angle.

Experimental measurements were made using a single-longitudinal-mode dual-polarization laser, shown in Fig. 2. The 4-cm long Fabry-Perot resonator incorporated a 2-mm long 1%-doped (111)-cut Nd:YAG gain crystal; a 21-mm long *z*-cut lithium niobate electro-optic crystal; a 30% partially reflecting 0.5-mm long etalon (for single longitudinal mode operation); a planar input mirror and a 15-cm radius of curvature output mirror ($R = 97\%$). The resonator mirrors were dielectric-coated (high reflectivity at 1.064 µm and transmissive at the pump wavelength) for single-pass longitudinal pumping. The pump source, an 808 nm fiber-coupled diode laser was polarized and focused into the gain crystal with a spot size of ~200 µm. The absorbed pump power was 1.2 to 1.5 times the laser threshold level for single longitudinal mode operation. A rotatable half waveplate controlled the pump polarization angle. Crystal mounting stresses were minimized to avoid birefringence. A small voltage was applied across the lithium niobate crystal to control the laser polarization axes, resulting in two orthogonal linear polarizations with a small optical frequency difference of ~150 MHz. The single-transverse-mode output of the dual-polarization laser was split into two paths using a polarizing beam splitter and thermal-based power meters measured the polarized power in each path. Amplified fast photodiodes monitored the transient dynamics of each polarization. For the same single crystal angle as shown in Fig. 1(c,d), the pump polarization controlled the laser output power in each polarization direction, giving excellent agreement with the rate-equation model. In addition, the output power variations with pump laser polarization angles

are consistent with those observed in Refs [15–17, 24] but experimental tests of the power dependence on the crystal angle are not practical due to the small power variation predicted.

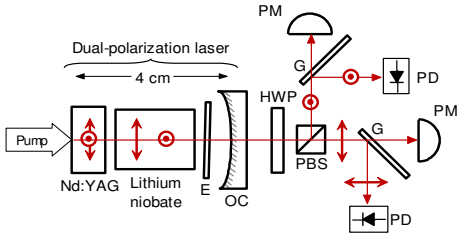

Fig. 2. Measurement arrangement of the polarized outputs (see Fig. 1) and polarization dynamics (see Fig. 3) of the dual-polarization laser. *E* is an etalon; OC laser output mirror; HWP is a half-waveplate; PBS is a polarization beam splitter; G are glass slides reflecting ~4%; PM are optical power meters; and PD are >1 MHz bandwidth photodiodes.

3. Relaxation oscillation frequencies

Small-signal dynamical behavior can be studied using linearized rate equations. In most solid-state lasers, the population-inversion lifetime is long compared to the photon lifetime, and typical RO frequencies exceed the inverse of the population inversion lifetime. Neglecting slow population-inversion decay rates, we obtain the characteristic equation:

$$\begin{vmatrix} s^2+\sum_{i=1}^{N}\frac{2\sigma_x^i\phi_{xst}l}{t_r}\gamma c\sigma_x^i n_{st}^i & \sum_{i=1}^{N}\frac{2\sigma_x^i\phi_{xst}l}{t_r}\gamma c\sigma_y^i n_{st}^i \\ \sum_{i=1}^{N}\frac{2\sigma_y^i\phi_{yst}l}{t_r}\gamma c\sigma_x^i n_{st}^i & s^2+\sum_{i=1}^{N}\frac{2\sigma_y^i\phi_{yst}l}{t_r}\gamma c\sigma_y^i n_{st}^i \end{vmatrix}=0, \tag{6}$$

where s is the Laplace variable and the subscript st implies the steady-state value of the annotated variable. The relations between the two RO frequencies ω_L, ω_R, (where $\omega_L \le \omega_R$) were obtained by solving Eq. (6) with $s^2=-\omega_{L,R}{}^2$ to give

$$\omega_L^2+\omega_R^2 \approx \sum_{i=1}^{N}\left(G_x^i\,\Gamma_x^i+G_y^i\,\Gamma_y^i\right) \tag{7}$$

$$\omega_L^2\cdot\omega_R^2 \approx \sum_{\{i,j\}}^{N}\left(G_x^i\,G_y^j-G_y^i\,G_x^j\right)\left(\Gamma_x^i\,\Gamma_y^j-\Gamma_y^i\,\Gamma_x^j\right) \tag{8}$$

where the set $\{i,j\}$ for Nd:YAG is defined by the k-subset of a set of 6 elements containing exactly 2 elements. The temporal gain (increasing photon density) due to the i-th atomic group is given by $G_x^i=\left(2n_{st}^i\sigma_x^i\right)/\tau_r$ for the x-polarized beam and $\Gamma_x^i=\gamma c\sigma_x^i\phi_{xst}$ is the population inversion decay rate by stimulated emission into the x-polarized beam. The modeled RO frequencies are plotted in Fig. 3(a,b). An analytical solution for the RO frequencies is

$$\omega_L^2+\omega_R^2 \approx \sum_{i=1}^{N}\frac{r^i-1}{\tau_s}\left(\frac{\alpha_x^i}{\tau_{px}^i}+\frac{\alpha_y^i}{\tau_{py}^i}\right). \tag{9}$$

Here r^i is the related to the pumping rate by $\Lambda^i=r^i n_{st}/\tau_s$ and $1/\tau_s$ is the sum of the population inversion decay rates due to stimulated emission into the x- and y-polarizations. This is explicitly given by $\tau_s=1/\left(\Gamma_x^i+\Gamma_y^i\right)$. The photon lifetime components are $\tau_{px}=1/G_x^i$, and the normalized stimulated emission cross-section factors are defined as $\alpha_x^i\equiv\phi_{xst}\sigma_x^i/\left(\phi_{xst}\sigma_x^i+\phi_{yst}\sigma_y^i\right)$ and $\alpha_y^i\equiv\phi_{yst}\sigma_y^i/\left(\phi_{xst}\sigma_x^i+\phi_{yst}\sigma_y^i\right)$ respectively. Neglecting the gain and pump polarization anisotropy, Eq. (9) reduces to the RO frequency relationship for a single-mode laser [27].

Refs [15–17] discuss the impact of pump polarization on the ROs but without considering the crystal angle and pump-polarization. We previously studied both pump-polarization and crystal-orientation effects in a (100)-cut Nd:YAG dual-polarization laser [7]. This cut of

Nd:YAG is weakly biaxial, switching between regions where a single polarization dominates because of strong gain anisotropy, and others with dual-polarization oscillations. However, the standard (111)-cut Nd:YAG has more subtle low-frequency dynamics. The in-phase (or McCumber) RO frequency (ω_R) calculated from RIN spectra [7], and shown in Fig. 3(a), is almost constant (less than 1% fluctuation) as pump polarization and crystal angle are varied, and is proportional to the square-root of pump power. The anti-phase RO (ω_L, see Fig. 3(b)) varies robustly as a function of both pump and crystal angles. The anti-phase RO shows a stronger dependence on the crystal angle (than the in-phase RO) because of the stimulated emission and gain anisotropy from each group (or crystallography site) of atoms. The experimental anti-phase RO frequencies (red squares in Fig. 3(c)) demonstrate excellent agreement despite the effect of power fluctuations on ω_R measurements. The crystal angle was set to ~35° with respect to the YAG unit cell in Fig. 3(c) and (d). Fig. 3(d) shows the experimentally measured mode-coupling constant (ratio of RO frequencies – see [9]) as a function of pump polarization angle at fixed crystal angle and low output power as in Fig. 1. The coupling constant depends on the self- and cross-saturation coefficients used in Lamb's analysis [12] and defines simultaneity and bistability regimes [9]; serving as a figure of merit [6,7] in dual-polarization lasers. The ratio of the RO frequencies depends on the crystal anisotropy. The effect of anisotropy on the fast dynamics shows the importance of crystal angle. For example, if the gain crystal was rotated by 30° then the trends shown in Fig. 1(c,d) remain the same but the anti-phase RO frequencies and the mode coupling in Fig. 3(c,d) appear as if pumped by the orthogonal polarization.

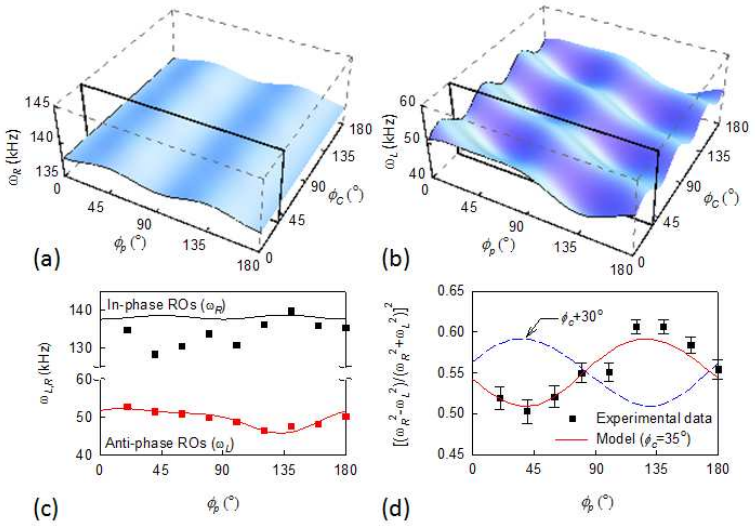

Fig. 3. Modeled (a) in-phase and (b) anti-phase RO frequency for a dual-polarization Nd:YAG laser pumped near threshold as a function of crystal angle (ϕ_c) and relative pump angle (ϕ_p). Corresponding (c) experimental in- and anti-phase RO frequencies and (d) Mode-coupling constant ($C = [(\omega_R^2-\omega_L^2)/(\omega_R^2+\omega_L^2)]^2$) as a function of pump polarization angle.

In conclusion we have developed an anisotropic rate equation model for solid-state lasers, and demonstrated its application in (111)-cut Nd:YAG. It shows that anisotropic atom-laser interactions lead to two RO frequencies which offer insights into polarization mode coupling. The model was used to explain gain and output power anisotropies, which depend on pump laser polarization angle and laser crystal orientation. Conversely, the measured anisotropies (i.e., the measured polarized output powers and the in- and anti-phase ROs) could also be used with the model to estimate the laser crystal orientation and atom-laser interaction anisotropy.